Characterization of the Binding Interface between the E-Domain of *Staphylococcal* Protein A and an Antibody Fv-Fragment†

David P. Meininger,‡ Mark Rance,§ Melissa A. Starovasnik,‡ Wayne J. Fairbrother,*,‡ and Nicholas J. Skelton*,‡

Department of Protein Engineering, Genentech, Inc., One DNA Way, South San Francisco, California 94080, and Department of Molecular Genetics, Biochemistry and Microbiology, University of Cincinnati College of Medicine, 231 Bethesda Avenue, Cincinnati, Ohio 45267

Received August 27, 1999

ABSTRACT: *Staphylococcal* protein A (SpA) is a cell-surface component of *Staphylococcus aureus*. In addition to the well-characterized interaction between SpA and the Fc-region of human IgG, an alternative binding interaction between SpA and the Fab-region of immunoglobulin domains encoded by the V_H3 gene family has been described. To characterize structurally the interface formed by SpA repeats and type-3 V_H-domains, we have studied the 32-kDa complex formed between an E-domain mutant (EZ4) and the Fv-fragment of the humanized anti-HER2 antibody (Hu4D5−8) using heteronuclear NMR spectroscopy. Protocols were established for efficient incorporation of ^{15}N, ^{13}C, and ^{2}H into EZ4 and the V_H- and V_L-domains of the Fv, allowing backbone resonances to be assigned sequentially for EZ4 and the V_H-domain in both free and complexed states. Broadening of certain V_H-resonances in the free and bound Fv-fragment suggests microsecond to millisecond time-scale motion in CDR3. Residues experiencing significant chemical shift changes of backbone $^{1}H^{N}$, ^{15}N, and ^{13}CO resonances upon complex formation delineate contiguous surfaces on EZ4 and the V_H-domain that define the binding interfaces of the two proteins. The interaction surfaces identified by chemical shift mapping are comprised of predominantly hydrophilic residues. This is in contrast to the SpA−Fc interface which is predominantly hydrophobic in nature. Further analysis of the surface properties suggests a probable binding orientation for SpA- and V_H3-domains.

Staphylococcal protein A (SpA) is a cell-surface component of the bacterial pathogen *Staphylococcus aureus*. The extracellular portion of SpA contains five homologous Ig-binding domains designated E, D, A, B, and C from the N-terminus. All five domains bind to the Fc-portion of human IgG1, IgG2, IgG3 allotype G3m(s,t) and IgG4 (*1*−*3*) and to the Fab-portion of certain IgG, IgA, IgM, and IgE sequences containing V_H-domains derived from the V_H3-family of gene segments (*4*−*7*). The majority of human peripheral B-cells normally presents membrane-bound IgM that contains a V_H3-domain; IgM cross-linking through the Fab-mediated interaction with SpA is known to induce B-cell mitogenesis in vitro. SpA has therefore been described as a B-cell superantigen (*8*). Additionally, the interaction of SpA with soluble IgG in plasma produces immune complexes that stimulate activation of the classical complement cascade, a response that is also known to require the Fab-binding ability of SpA (*9*, *10*).

Isolated domains of SpA have been the subject of several structural studies. In particular, the solution structures have been determined for E- (*11*), B- (*12*), and Z-domains (*13*) [where Z-domain designates a B-domain variant (*14*) that binds Fc- but not Fab-fragments (*7*)]. The isolated SpA-domains comprise three α-helices that pack together to form a compact helical-bundle. The structure of the complex between B-domain and the Fc-fragment of IgG has also been determined by X-ray crystallography (*15*). Residues in helices 1 and 2 of B-domain interact with Fc-residues proximal to the C_H2-C_H3 interface. The contact residues are predominantly hydrophobic in nature.

The SpA−Fab interface is not well characterized. However, the SpA-binding site is located clearly within a region of the V_H3-domain outside the V_H-V_L interface and the conventional antigen-binding site, since the presence or absence of V_L-domain or most antigens does not affect binding (*16*, *17*). Backbone NMR assignments have been reported for an isolated V_H3-domain (modified by mutating three residues at the V_H-V_L interface in order to improve solubility) (*18*). Changes in backbone chemical shifts upon binding a SpA-construct containing domains A and B led these authors to propose that SpA binding involves the surface formed by β-sheet 1 of the V_H3-domain. Framework regions 1 (FR1) and 3 (FR3), which include residues in β-sheet 1, as well as the C-terminal region of CDR2 have also been implicated in SpA binding based on sequence

† M.R. was supported for this work by the National Institutes of Health (GM40089).

* To whom correspondence should be addressed. (N.J.S.) Phone: (650) 225-6402. Fax: (650) 225-3734. E-mail: skelly@gene.com. (W.F.J.) Phone: (650) 225-6372. Fax: (650) 225-3734. E-mail: fairbro@gene.com.

‡ Genentech, Inc.

§ University of Cincinnati College of Medicine.

[1] Abbreviations: CDR, complementarity determining region; EDTA, ethylenediaminetetraacetic acid; EZ4, protein A E-domain mutant (V14I, D23E, G44A, S52A); FR, framework region; MALDI, matrix-assisted laser desorption; NOE, nuclear Overhauser effect; PMSF, phenylmethanesulfonyl fluoride; SpA, *Staphylococcal* protein A; TPPI, time-proportional-phase-incrementation.

10.1021/bi9920174 CCC: $19.00
Published on Web 12/08/1999

comparisons (*19*−*22*) and swap mutations (*23*, *24*) between SpA-binding and non-SpA-binding V_H-sequences. Additionally, the V_H-binding site on E-domain was shown by chemical shift mapping to involve residues in helices 2 and 3 (*16*). In both this and the previously mentioned NMR study of the isolated V_H3-domain, binding sites were deduced without completing chemical shift assignments for the bound states.

We have used NMR spectroscopy to investigate the complex formed between a mutant of SpA domain E (EZ4) and an Fv-fragment derived from a humanized anti-HER2 antibody (*25*). The E-domain mutant contains E-to-Z (or B) substitutions V14I, D23E, G44A, and S52A [E-domain sequence numbering is as described previously (*11*)] that provide greatly increased thermal stability for the domain while not significantly affecting its affinity for Hu4D5 Fab (E. Zhukovsky, R. F. Kelley, and M. A. Starovasnik, unpublished results). Each of the three polypeptide chains in the EZ4−Fv complex have been expressed separately in *Escherichia coli*. Optimized expression and purification protocols allowed efficient production of these molecules with a variety of isotopic enrichments, including ^{15}N, $^{15}N/^{13}C$, and $^{15}N/^{13}C/^{2}H$ for both EZ4 and V_H and ^{2}H for V_L. Backbone $^{1}H^{N}$, ^{15}N, and ^{13}C resonance assignments have been completed for EZ4 and the V_H-domain of the Fv-fragment both free in solution and in the ternary 32 kDa EZ4−Fv complex. Resonances of both proteins undergo chemical shift changes upon complex formation; residues experiencing the most significant chemical shift changes are localized to distinct surfaces of EZ4 and the V_H-domain, thus allowing identification of the binding interface.

MATERIALS AND METHODS

Materials. D_2O (99.9% D) was purchased from Cambridge Isotopes Laboratories. Isotopically enriched [$^{13}C_6$]-D-glucose (>99%), [$^{2}H_7$]-D-glucose (>97%), [$^{13}C_6$, $^{2}H_7$]-D-glucose (>98% ^{13}C, >97% ^{2}H), [^{15}N]ammonium chloride (>99%), Celtone-U, Celtone-N, and Celtone-CN were purchased from Martek, Inc.

Protein Expression. Protonated EZ4 was expressed under the regulation of the alkaline phosphatase (*phoA*) promoter and was secreted into the periplasm of a protease deficient mutant of *E. coli* strain W3110 as directed by the STII signal sequence (*26*). Production of ^{15}N-labeled and $^{15}N/^{13}C$-labeled protein was carried out as described previously (*27*), except that upon completion of the growth phase cell pellets were washed in 1/2 vol of fresh media lacking ammonium chloride, glucose, and Celtone. The cells were subsequently resuspended in a volume of production media, or growth media lacking Celtone (which is the sole phosphate source) equivalent to the original volume of growth media.

The Hu4D5−8 V_H- and V_L-domains, as well as deuterated EZ4, were expressed under the regulation of the *taq* promoter and secreted into the periplasm of a mutant of *E. coli* strain K12 through inclusion of the STII signal sequence (*26*). Protein production using this system was found generally to be higher in low-density fermentations than in shaker flasks; therefore, cultures were grown in a BioFlow III (New Brunswick) fermentor. Fermentations were carried out in a volume of 1.5−2.0 L at 37 °C, pH 7.0, with an agitation rate of 500 rpm and an air flow rate of 5 L/min. The basal fermentation media consisted of M9 minimal media containing 2 g/L glucose and 0.8 g/L NH_4Cl, supplemented with 1.6 mg/L thiamine. An additional 3 g/L glucose, 1.2 g/L NH_4Cl, and 2.4 mg/L thiamine was delivered via a solution fed during induction at a rate incremented such that minimal NaOH was required to maintain a steady-state pH of 7.0. Deuterated protein production began with the following D_2O cell conditioning process: a starter culture was grown at 37 °C in LB media to an A_{600} of ∼0.6 and then diluted 40-fold into a small volume of 90% D_2O M9 media containing 100% protonated glucose. At an A_{600} of ∼1.8, the culture was diluted 100-fold into M9 media deuterated to the extent desired for the protein being produced. A drying column was included in the air input line during deuterated fermentations to minimize the introduction of air-born water to the culture. Growth rates were typically ∼50% slower and final cell densities ∼15% lower in perdeuterated fermentations compared to protonated fermentations.

Table 1: Yields of Purified Components of the EZ4−Fv Complex

	promoter	yield (mg/L culture)
^{1}H V_H + ^{1}H V_L[a]	*taq*	50
$^{15}N/^{13}C/^{1}H$ V_H + ^{2}H V_L[a]	*taq*	42
$^{15}N/^{13}C/^{2}H$ V_H + ^{2}H V_L[a]	*taq*	30
^{1}H EZ4	*phoA*	180
$^{1}H/^{15}N$ EZ4	*phoA*	180
$^{15}N/^{13}C/^{1}H$ EZ4	*phoA*	220
$^{15}N/^{13}C/^{2}H$ EZ4	*taq*	22

[a] Yields represent the amount of Fv obtained from 1 L of V_H-culture plus 1 L of V_L-culture.

Protein Purification. Expression driven by either the *phoA* or *taq* promoter did not lead to the accumulation of significant amounts of protein in the culture media. Purification of EZ4 was therefore as described previously for E-domain (*11*) except that the only source of protein was the periplasmic shockate. Affinity-purified protein was further purified and simultaneously buffer exchanged through size-exclusion chromatography. Protein was >95% pure as determined by SDS−PAGE and was verified to have the correct molecular mass via MALDI mass spectrometry. Yields of purified EZ4 are listed in Table 1.

The V_H-domain readily forms homodimers and higher order aggregates when purified alone. Improved yields were obtained when cell pellets containing V_H and V_L derived from separate fermentations were resuspended together (∼250 g/L) in ice-cold 10 mM Tris buffer, pH 7.5, containing 1 mM EDTA and 0.1 mM PMSF, and the two domains copurified as the Fv-fragment. The resulting suspension was stirred at 4 °C for 30 min and then centrifuged. The periplasmic shockate was then loaded directly onto a protein A-Sepharose 4 Fast Flow column (Pharmacia). The desired heterodimeric protein was subsequently separated from homodimeric V_H (20−25%) and high molecular weight aggregates (<5%) and buffer exchanged using size-exclusion chromatography. The resulting Fv-fragment was >95% pure as determined by SDS−PAGE and the molecular mass was verified via MALDI mass spectrometry. Yields of purified Fv are listed in Table 1.

EZ4 samples contained 0.5−1.5 mM EZ4 and, in the case of samples of the complex, ∼50% excess Fv. V_H-samples contained 1.0−1.5 mM Fv and, in samples of the complex, ∼50% excess EZ4. Protein concentrations were verified

Table 2: Acquisition Parameters for NMR Experiments Performed on the EZ4−Fv complex

experiment	acquired data matrix[a] (nucleus) t_1	t_2	t_3	spectral widths (Hz) F_1	F_2	F_3	no. of transients	ref
$^{15}N/^{13}C$-labeled EZ4								
^{15}N-HSQC[b]	128 (^{15}N)	2048 (^{1}H)		1562.5	12 500		16	*55*
HNCO[b]	32 (^{13}CO)	32 (^{15}N)	2048 (^{1}H)	1509.2	1500	8012.8	32	*36*
HN(CO)CA[b]	32 ($^{13}C^{\alpha}$)	32 (^{15}N)	2048 (^{1}H)	3125	1500	8012.8	32	*56*
HNCA[b]	32 ($^{13}C^{\alpha}$)	32 (^{15}N)	2048 (^{1}H)	3125	1500	8012.8	32	*56*
(H)C(CO)NH-TOCSY[b]	64 (^{13}C)	32 (^{15}N)	1024 (^{1}H)	6800.4	1250	6250	32	*57, 58*
$^{15}N/^{13}C/^{2}H$-labeled EZ4								
^{15}N-HSQC[b]	128 (^{15}N)	2048 (^{1}H)		1562.5	12 500		16	*55*
HNCO[b]	32 (^{13}CO)	20 (^{15}N)	2048 (^{1}H)	1509.2	925.9	8012.8	16	*36*
HNCA[b]	32 ($^{13}C^{\alpha}$)	22 (^{15}N)	2048 (^{1}H)	3125	925.9	8012.8	16	*59*
HN(COCA)CB[b]	42 ($^{13}C^{\beta}$)	24 (^{15}N)	2048 (^{1}H)	5451.4	1087	6250	32	*60*
$^{15}N/^{13}C/^{2}H$-labeled EZ4 + unlabeled Fv								
^{15}N-HSQC[b]	150 (^{15}N)	2048 (^{1}H)		1500	12 500		16−64	*55*
HNCO[b]	32 (^{13}CO)	20 (^{15}N)	2048 (^{1}H)	1509.2	925.9	8012.8	64	*36*
HN(CA)CO[b]	32 (^{13}CO)	20 (^{15}N)	2048 (^{1}H)	1509.2	925.9	8012.8	192	*61*
HN(CO)CA[b]	32 ($^{13}C^{\alpha}$)	22 (^{15}N)	2048 (^{1}H)	3125	925.9	8012.8	64	*60*
HNCA[b]	32 ($^{13}C^{\alpha}$)	22 (^{15}N)	2048 (^{1}H)	3125	925.9	8012.8	96	*59*
HN(COCA)CB[b]	42 ($^{13}C^{\beta}$)	20 (^{15}N)	2048 (^{1}H)	6273.5	925.9	8012.8	128	*60*
HN(CA)CB[b]	42 ($^{13}C^{\beta}$)	20 (^{15}N)	2048 (^{1}H)	6273.5	925.9	8012.8	160	*60*
^{15}N-NOESY-HSQC[c,d]	88 (^{1}H)	40 (^{15}N)	2048 (^{1}H)	9090.9	1785.7	12500	16	*62*
$^{15}N/^{13}C/^{2}H$-labeled V_H + ^{2}H-labeled V_L								
^{15}N-HSQC[b,e]	150 (^{15}N)	2048 (^{1}H)		1500	12 500		8−64	*55*
HNCO[e]	32 (^{13}CO)	32 (^{15}N)	2048 (^{1}H)	1509.2	1500	8064.5	32	*36*
HN(CA)CO[e]	31[f] (^{13}CO)	32 (^{15}N)	2048 (^{1}H)	1509.2	1500	8064.5	64	*61*
HN(CO)CA[e]	32 ($^{13}C^{\alpha}$)	32 (^{15}N)	2048 (^{1}H)	3125	1519.8	8064.5	32	*60*
HNCA[e]	32 ($^{13}C^{\alpha}$)	32 (^{15}N)	2048 (^{1}H)	3125	1519.8	8064.5	16	*59*
HN(COCA)CB[e]	48 ($^{13}C^{\beta}$)	24 (^{15}N)	2048 (^{1}H)	6273.5	1519.8	8064.5	32	*60*
HN(CA)CB[e]	46[f] ($^{13}C^{\beta}$)	32 (^{15}N)	2048 (^{1}H)	6273.5	1519.8	8064.5	32	*60*
$^{15}N/^{13}C$-labeled V_H + ^{2}H-labeled V_L								
^{15}N-HSQC[e]	150 (^{15}N)	2048 (^{1}H)		1500	12 500		8−64	*55*
HNCO[e]	18[f] (^{13}CO)	32 (^{15}N)	2048 (^{1}H)	1509.2	1500	8064.5	32	*36*
HN(CO)CA[e]	32 ($^{13}C^{\alpha}$)	32 (^{15}N)	2048 (^{1}H)	3125	1519.8	8064.5	32	*60*
HNCA[e]	32 ($^{13}C^{\alpha}$)	32 (^{15}N)	2048 (^{1}H)	3125	1519.8	8064.5	16	*59*
CB(CACO)NH[b]	32 ($^{13}C^{\beta}$)	32 (^{15}N)	2048 (^{1}H)	7541.5	1519.8	6250	32	*36*
$^{15}N/^{13}C/^{2}H$-labeled V_H + ^{2}H-labeled V_L + unlabeled EZ4								
^{15}N-HSQC[b]	128 (^{15}N)	4096 (^{1}H)		1562.5	12 500		64−128	*55*
HNCO[b]	32 (^{13}CO)	32 (^{15}N)	2048 (^{1}H)	1509.2	1500	8012.8	64	*56*
HN(CO)CA[b]	28 ($^{13}C^{\alpha}$)	28 (^{15}N)	2048 (^{1}H)	3125	1500	8012.8	128	*60*
HNCA[b]	28 ($^{13}C^{\alpha}$)	28 (^{15}N)	2048 (^{1}H)	3125	1500	8012.8	128	*59*
TROSY-HNCO[c]	120 (^{13}CO)	50 (^{15}N)	1376 (^{1}H)	1509.2	2000	15625	64	*38*
TROSY-HN(COCA)CB[g]	28 ($^{13}C^{\beta}$)	28 (^{15}N)	1216 (^{1}H)	3125	1666.7	12500	128	*39, 60*
TROSY-HN(CA)CB[g]	28 ($^{13}C^{\beta}$)	28 (^{15}N)	1216 (^{1}H)	3125	1666.7	12500	128	*39, 60*
^{15}N-NOESY-HSQC[c,h]	128 (^{1}H)	46 (^{15}N)	2752 (^{1}H)	9090.9	2604.2	15625	8	*62*

[a] Complex data points. [b] Data acquired on a Bruker DRX 500 MHz spectrometer. [c] Data acquired on a Varian Inova 800 MHz spectrometer. [d] Mixing time, 100 ms. [e] Data acquired on a Bruker AMX 500 MHz spectrometer. [f] Acquisition ended prematurely due to hardware failure. [g] Data acquired on a Varian Inova 600 MHz spectrometer. [h] Mixing time, 90 ms.

through amino acid analysis. Levels of isotopic enrichment were verified through MALDI mass spectrometry. ^{15}N labeling was >99%; ^{13}C labeling was >99% in $^{15}N/^{13}C-$EZ4 or $^{15}N/^{13}C-V_H$ and >98% in $^{15}N/^{13}C/^{2}H$-EZ4 or $^{15}N/^{13}C/^{2}H-V_H$. ^{2}H-labeling was >99% in perdeuterated-V_L, >95% in deuterated-EZ4, and >90% in deuterated-V_H. All NMR samples contain 50 mM sodium phosphate, pH 5.7, 15−25 mM NaCl, ~0.1 mM EDTA, 0.02% sodium azide, and 92% H_2O/8% D_2O.

NMR Spectroscopy. All NMR spectra were acquired at 35 °C. Most spectra were acquired on either a Bruker AMX500 or DRX500 spectrometer equipped with Bruker 5-mm inverse triple-resonance probes with three-axis gradient coils. Additionally, several experiments were acquired on either 600 or 800 MHz Varian Inova spectrometers equipped with Varian 5-mm inverse triple-resonance probes with three-axis gradient coils. Proton chemical shifts were referenced to internal 3-(trimethyl-silyl)propane-1,1,2,2,3,3-d_6-sulfonic acid, sodium salt (DSS-d_6; Isotec) and ^{15}N and ^{13}C chemical shifts were referenced indirectly to liquid ammonia and DSS, respectively (*28*). Backbone $^{1}H^{N}$, ^{15}N, and ^{13}C resonances were assigned sequentially using through-bond heteronuclear correlation experiments (*29*); experimental details are summarized in Table 2. Quadrature detection in the indirectly detected dimensions was achieved using the States-TPPI method (*30*). Solvent suppression in the ^{15}N-HSQC experiments was achieved using the water "flip-back" method (*31*). In the ^{15}N-NOESY-HSQC experiments, solvent suppression was achieved via binomial excitation (*32*), with appropriate modifications to minimize the deleterious effects of radiation damping of the water signal (*33, 34*). Triple resonance experiments included ^{15}N coherence selection via pulsed field gradients (*35, 36*), except for those acquired at 600 or 800 MHz, which were modified to include the TROSY scheme with sensitivity enhancement and water flip-back (*37*−*39*). ^{1}H and ^{2}H broad-band decoupling was achieved using the WALTZ-16 sequence (*40*) where appropriate while GARP-1 (*41*) was used for ^{15}N decoupling during acquisition. $^{13}C^{\alpha}$ and ^{13}CO decoupling was achieved through either selective 180° pulses or SEDUCE-1 composite pulse decoupling (*42, 43*). All spectra were processed and analyzed on a Silicon Graphics Indigo 2 workstation using the FELIX 97.0 software package.

RESULTS

Choice of E-Domain Construct. Previous studies indicated that wild-type E-domain has a low thermal stability (T_m = 43 °C) and a propensity to aggregate and form a highly viscous gel after several hours at millimolar concentration and 35 °C (*11, 16*). Z-domain [the G27A mutant of B-domain

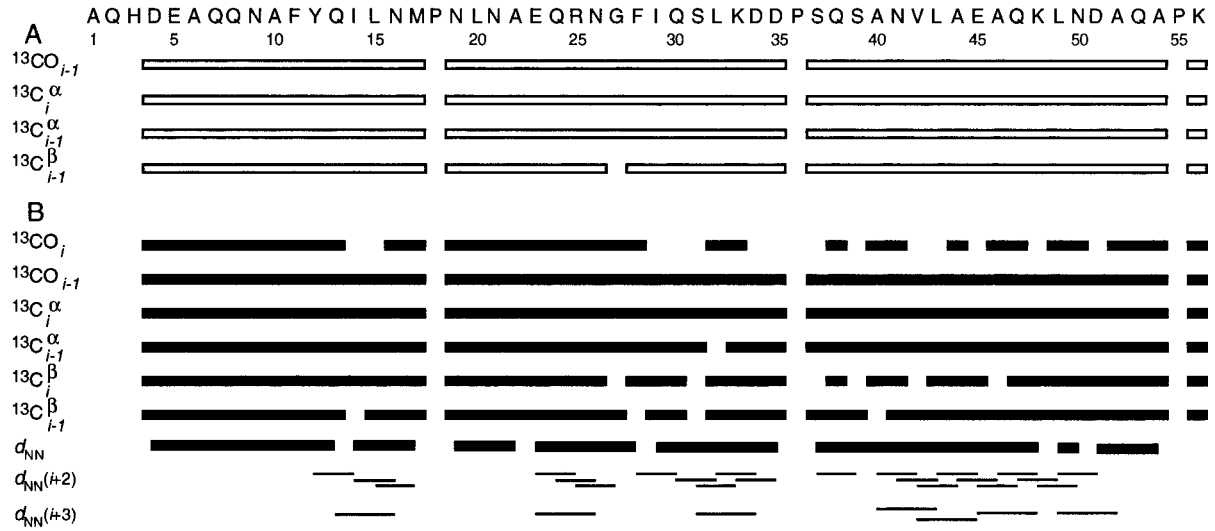

FIGURE 1: Schematic representation of the backbone correlations observed for free (A, open) and Fv-bound (B, filled) EZ4. The presence of a cross-peak for a given residue is indicated by a bar. The correlations are found in the following spectra: $^{13}CO_i$, HN(CA)CO; $^{13}CO_{i-1}$, HNCO; $^{13}C_i^{\alpha}$, HNCA; $^{13}C_{i-1}^{\alpha}$, HN(CO)CA and/or HNCA [and/or (H)C(CO)NH-TOCSY (A)]; $^{13}C_i^{\beta}$, HN(CA)CB; $^{13}C_{i-1}^{\beta}$, (H)C(CO)NH-TOCSY (A) or HN(COCA)CB (B); d_{NN}, $^1H^N-^1H^N$ sequential and medium-range NOE correlations from ^{15}N-NOESY-HSQC of Fv-bound EZ4. Side-chain correlations observed in the (H)C(CO)NH-TOCSY spectrum of free EZ4 are not shown.

(*14*)] does not exhibit this behavior, but it also does not bind Fv. Four of 11 possible E-to-Z substitutions (V14I, D23E, G44A, and S52A) were incorporated into E-domain (E. Zhukovsky, R. F. Kelley, and M. A. Starovasnik, unpublished results). The resulting mutant protein, designated EZ4, has a higher thermal stability (T_m = 63 °C) and a reduced tendency to aggregate compared to wild-type E-domain while maintaining tight Fv-association [K_d = 12.5 ± 0.8 μM for EZ4 (R. F. Kelley, unpublished results) versus 5.0 ± 0.8 μM for E-domain (*16*)]. ^{1}H and ^{15}N chemical shifts of EZ4 are similar to those of wild-type E-domain, indicating that the three-helix-bundle structure (*11*) is likely maintained in the quadruple mutant. On the basis of these data, the EZ4-mutant, rather than the wild-type E-domain, was selected for further analysis.

Addition of substoichiometric amounts of unlabeled-Fv to ^{15}N-labeled EZ4 results in HSQC spectra that exhibit cross-peaks corresponding to both free and Fv-bound states in slow exchange, as observed previously with ^{15}N-labeled E-domain (*16*). Similarly, HSQC spectra acquired on samples containing ^{15}N-labeled-V_H, unlabeled-V_L, and substoichiometric amounts of unlabeled-EZ4 also produced two sets of resonances corresponding to free- and EZ4-bound states of Fv in slow exchange. The average $^1H^N$-line widths of the peaks in spectra of bound EZ4 in the presence of 50% excess Fv were 24 ± 4 Hz.

Backbone Resonance Assignments of Free and Fv-Bound EZ4. Samples containing ^{15}N/^{13}C-labeled EZ4 were used in the triple-resonance experiments listed in Table 2 to obtain backbone resonance assignments for free EZ4. Amide correlations for all nonproline residues, except the first three residues from the N-terminus, were observed in these experiments. The (H)C(CO)NH-TOCSY experiment allowed sets of $^1H^N$, ^{15}N, and ^{13}C resonances to be assigned to specific amino acid types. Data from this experiment, in combination with the HNCO, HNCA, and HN(CO)CA experiments, were sufficient to assign the backbone ($^1H^N$, ^{15}N, ^{13}CO, and $^{13}C^{\alpha}$) and $^{13}C^{\beta}$ resonances of all residues, except Ala1, Gln2, and His3 and the ^{13}CO resonances of residues N-terminal to

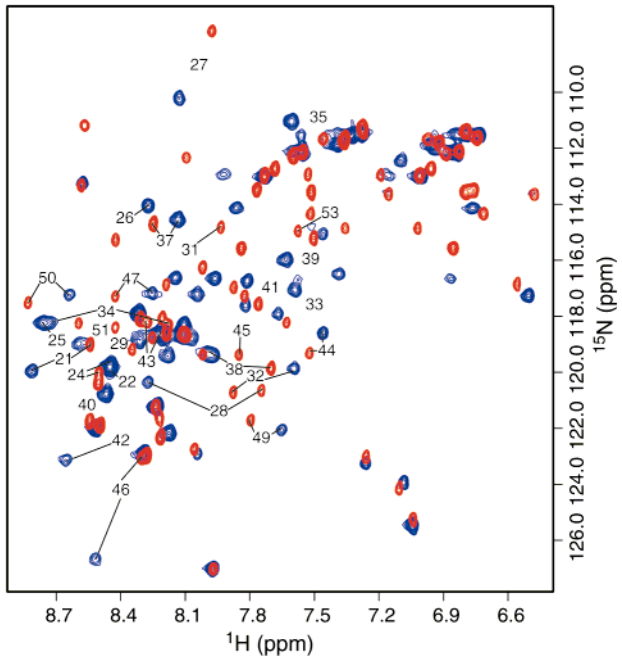

FIGURE 2: Superposition of 2D ^{1}H/^{15}N-HSQC spectra of free (red) and Fv-bound ^{15}N/^{13}C/^{2}H-labeled EZ4 (blue). The EZ4 concentration is ~1 mM in both states. Assignments for several peaks significantly perturbed upon Fv binding are indicated.

prolines. The observed correlations are summarized in Figure 1A.

Spectra were also acquired on ^{15}N/^{13}C/^{2}H-labeled EZ4 (Table 2) and assigned by inspection using assignments for the protonated protein. The two sets of resonance assignments were used to deduce ^{2}H-isotope-shifts for $^{13}C^{\alpha}$ and $^{13}C^{\beta}$ resonances.

^{15}N-HSQC spectra for free and Fv-bound EZ4 are shown superposed in Figure 2. The backbone resonances for Fv-bound EZ4 were assigned using the experiments listed in Table 2 collected on a sample containing ^{15}N/^{13}C/^{2}H-labeled EZ4 and excess unlabeled-Fv. Amide correlations for all nonproline residues, except the first three residues from the

N-terminus, were observed in two or more of these experiments. Rather weak correlations were observed, however, in the HN(CA)CO, HN(CA)CB, and HN(COCA)CB triple-resonance experiments acquired on Fv-bound EZ4 for a number of residues postulated previously to be involved in binding of E-domain to Fv (*16*); several of these resonances are broadened beyond detection. The correlations observed for Fv-bound EZ4 are summarized in Figure 1B. Backbone resonance assignments for the bound state of EZ4 were confirmed through observation of sequential $^1H^N-^1H^N$ NOEs in a ^{15}N-edited NOESY-HSQC spectrum (Figure 1B). In addition, all $i-i+2$ and $i-i+3$ $^1H^N-^1H^N$ distances less than 5 Å in a model of EZ4 [based on the solution structure of E-domain (*11*)] produced observable NOEs in the ^{15}N-edited NOESY-HSQC spectrum (the only exceptions involved resonance degeneracy or overlap with diagonal peaks) (Figure 1B), indicating that the helical secondary structure of the domain is preserved upon Fv-binding.

Complete lists of EZ4 backbone resonance assignments for the free and Fv-bound protein are provided in the Supporting Information (Table S1), together with plots showing deviations from random-coil chemical shift values for the assigned ^{13}CO, $^{13}C^{\alpha}$, and $^{13}C^{\beta}$ resonances (Figures S1 and S2). Consensus chemical shift index (CSI) values (*44*), based on these chemical shift differences, are shown in Figure 3, for EZ4 residues in the free and bound states, respectively. The consensus CSIs for the free and bound states are identical and are consistent with the helical secondary structure of SpA-domains. Note that the ^2H-isotope-shifts for the bound state could not be measured reliably due to the poor quality of the data observed for protonated, Fv-bound, EZ4 (data not shown); the bound-state chemical shift data presented in Figures S2 and 3B were corrected using the ^2H-isotope-shifts measured for the free-state.

V_H-Domain Backbone Resonance Assignments in the Free and EZ4-Bound Fv-Fragment. The Hu4D5−8 V_H-backbone resonances were assigned in the free Fv-fragment using the experiments listed in Table 2 acquired on a sample containing $^{15}N/^{13}C/^2H$-labeled V_H and perdeuterated-V_L. Amide resonances were assigned for 106 of the 117 nonproline V_H-residues. Additionally, 111 of 120 ^{13}CO resonances, 114 of 120 $^{13}C^{\alpha}$ resonances, and 94 of 105 $^{13}C^{\beta}$ V_H-resonances were assigned. The correlations observed for each residue in the triple-resonance spectra are summarized in Figure 4A. Ten of the 11 unobserved amide protons participate in cross-strand hydrogen bonds in the crystal structure of the domain (*45*), ruling out chemical exchange with solvent as an explanation for the lack of observable signal (the 11th is at the N-terminus). When mapped onto the X-ray structure of the domain, these residues form a distinct cluster, adjacent to the V_H-V_L interface, that includes sections of strand A from β-sheet 1 and strands C, F, and G from β-sheet 2 as illustrated in Figure 5. In addition, many resonances corresponding to residues within CDR3 are broadened significantly. A total of six crystallographically unique copies of the 4D5 V_H-domain structure are available; the largest deviation in conformation between the structures occurs in CDR3 (*45*), suggesting that conformational exchange involving CDR3 is the likely cause of the missing signals. This hypothesis is supported by the results of an NMR analysis performed on a single-chain Fv-fragment in which assignments were also lacking for similar regions of strands F and G (*46*); the authors suggest that the lack of information obtained for these regions may be due to an intrinsic dynamic property of CDR3. Exchange broadening of V_H-CDR3 amide resonances has also been reported for the Fv-fragment of a murine anti-dansyl IgG2a antibody (*47*).

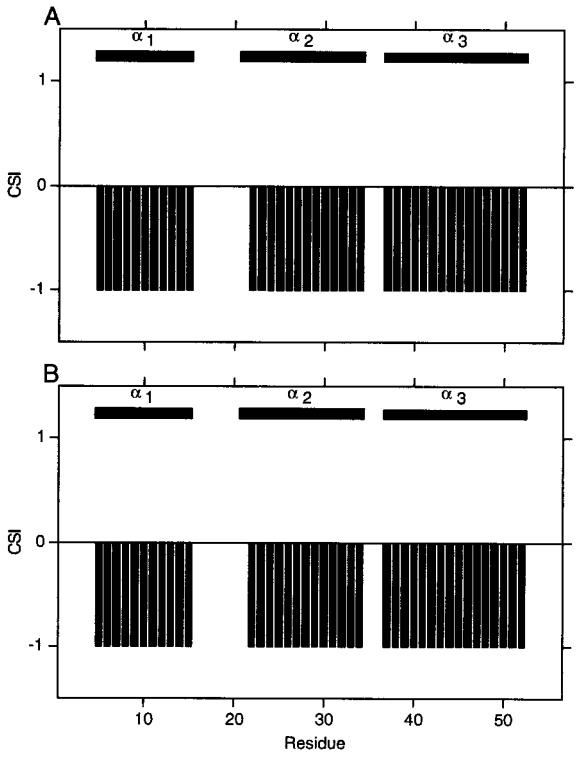

FIGURE 3: Consensus CSIs for free (A) and Fv-bound (B) EZ4. The secondary structure observed for free E-domain (*11*) is shown schematically at the top of each panel.

Experiments were also acquired on a sample containing $^{15}N/^{13}C$-labeled-V_H and perdeuterated-V_L as listed in Table 2. Resonances in these experiments were assigned by inspection and the assignments used to derive ^2H-isotope-shifts for the $^{13}C^{\alpha}$ and $^{13}C^{\beta}$ resonances of the V_H-domain. ^{15}N-HSQC spectra for the V_H-domain in the free and EZ4-bound Fv-fragment are shown superposed in Figure 6. Significant line width variations are evident in both spectra with average ^1H V_H-domain line widths of 17 ± 5 and 36 ± 7 Hz in the spectra of the free and EZ4-bound Fv-fragment, respectively. Backbone resonance assignments of the V_H-domain in the EZ4-bound Fv-fragment were obtained using the experiments listed in Table 2 acquired on a sample containing $^{15}N/^{13}C/^2H$-labeled-V_H and perdeuterated-V_L in the presence of excess unlabeled-EZ4. Preliminary V_H-backbone assignments of the EZ4-bound Fv were possible using only the HNCO, HNCA, and HN(CO)CA experiments, together with the V_H-assignments from the free Fv-fragment, because many residues did not experience significant changes in chemical shift upon formation of the complex. These preliminary assignments were confirmed through later analysis of the TROSY-type HN(CA)CB and HN(COCA)CB experiments collected at 800 MHz. Amide resonances for 80 of 117 nonproline V_H-domain residues were assigned in addition to 80 of 120 ^{13}CO, 93 of 120 $^{13}C^{\alpha}$, and 74 of 105 $^{13}C^{\beta}$ V_H-resonances. The V_H-domain correlations observed in triple-resonance experiments acquired on the EZ4-bound Fv-fragment are summarized in Figure 4B. Residues lacking

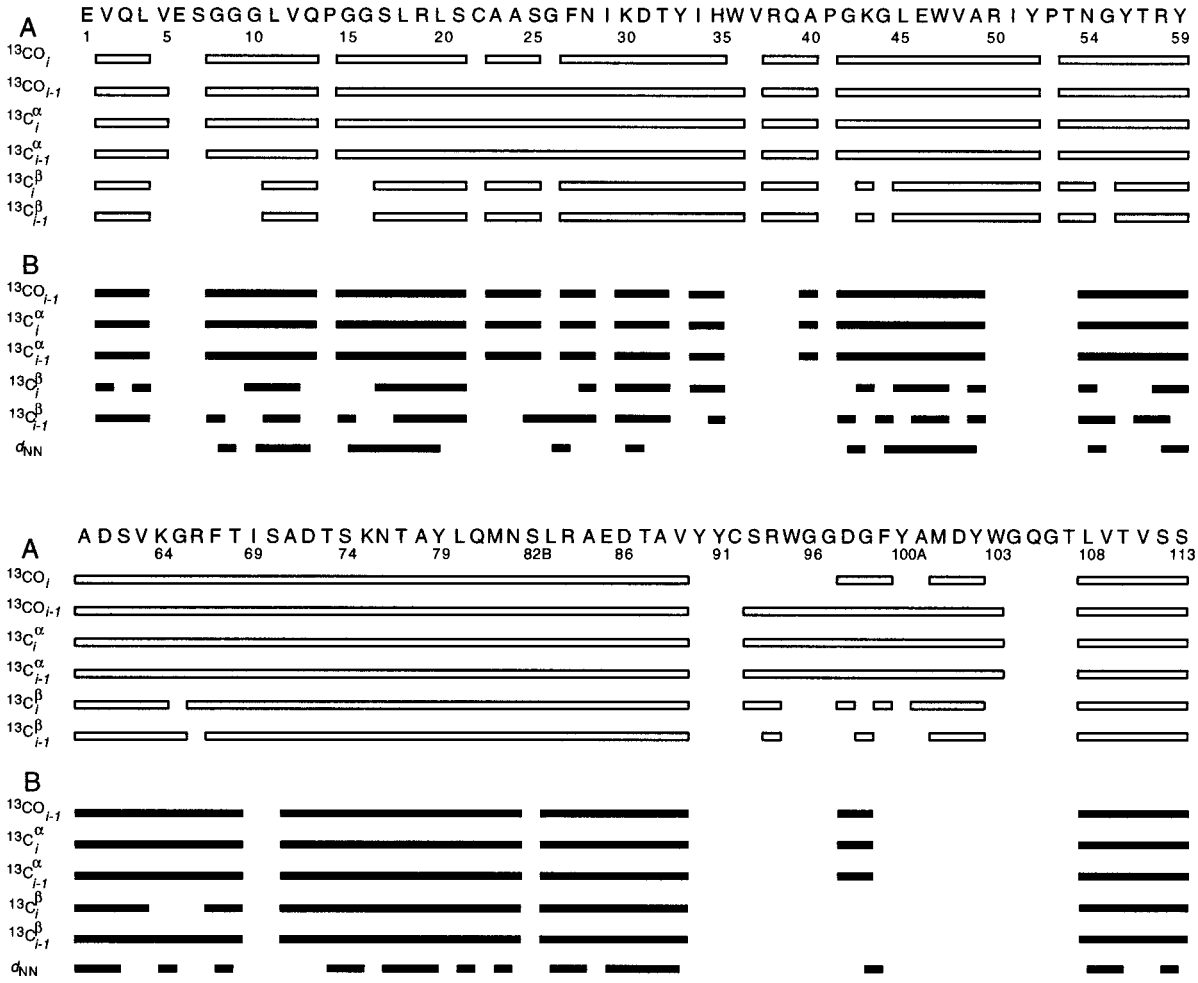

FIGURE 4: Schematic representation of the V_H-domain backbone correlations observed for free (A, open) and EZ4-bound (B, filled) Fv. The presence of a cross-peak for a given residue is indicated by a bar. The correlations are found in the following spectra: $^{13}CO_i$, HN(CA)CO; $^{13}CO_{i-1}$, HNCO; $^{13}C^{\alpha}_i$, HNCA; $^{13}C^{\alpha}_{i-1}$, HN(CO)CA, and/or HNCA; $^{13}C^{\beta}_i$, HN(CA)CB; $^{13}C^{\beta}_{i-1}$, HN(COCA)CB; d_{NN}, $^1H^N-^1H^N$ sequential NOE correlations from ^{15}N-NOESY-HSQC of EZ4-bound Fv.

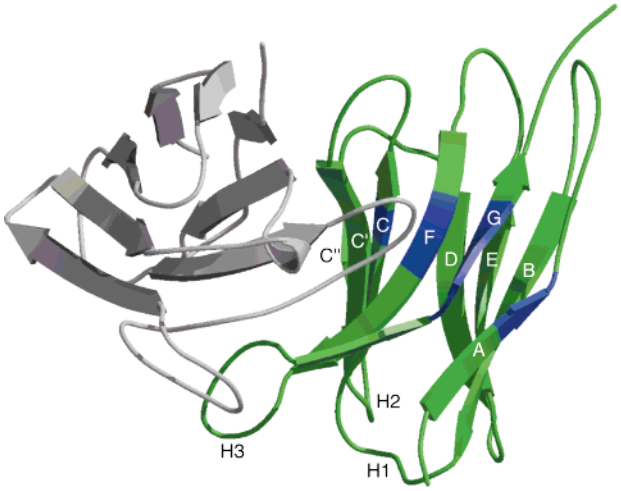

FIGURE 5: Schematic representation of the Fv crystal structure [PDB accession code 1FVC (*45*)] illustrating the locations of V_H-residues for which amide resonances were not observed in the free Fv-fragment (violet). The strands of the V_H-domain are labeled. The V_L-domain is shown in gray. This figure was generated using the program MOLSCRIPT (*63*).

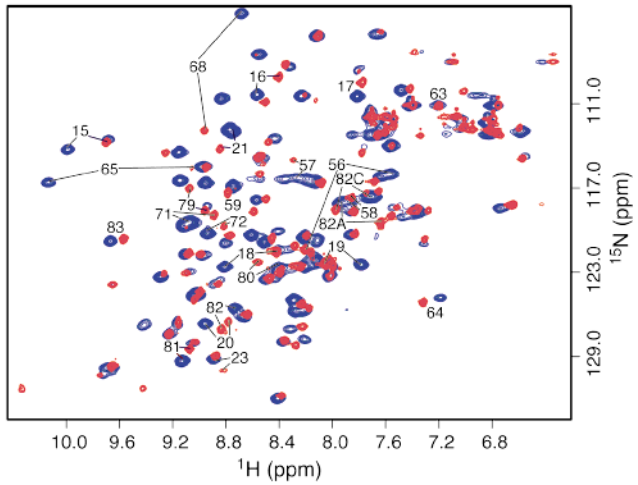

FIGURE 6: Superposition of 2D $^1H/^{15}N$-HSQC spectra of the V_H-domain in the free (red) and EZ4-bound (blue) $^{15}N/^{13}C/^2H$-labeled Fv-fragment. Both spectra were acquired on samples containing ~1.5 mM Fv. Assignments for several peaks significantly perturbed upon EZ4 binding are indicated.

observable amide resonances include all but two residues from CDR3 and, with the exceptions of Cys22, Ile69, Ser70, and Ser82B, form a contiguous region within the V_H-domain composed of residues within and proximal to CDR3, suggesting further that flexibility in this region of the domain is the primary origin of the observed linebroadening. Note that these resonances were already broadened significantly in the free Fv; their loss on complex formation is probably

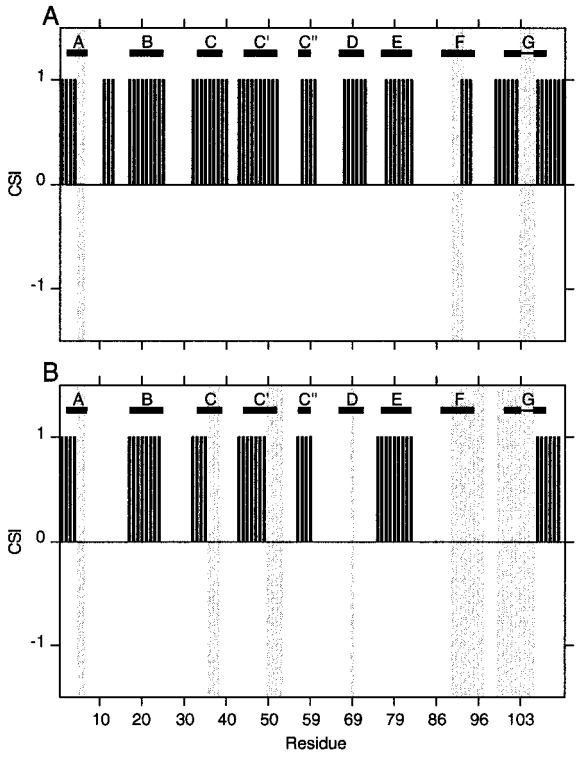

FIGURE 7: Consensus CSIs for V_H-residues in free (A) and EZ4-bound (B) Fv. The secondary structure observed in the crystal structures of the V_H-domain is shown schematically above each panel. Absence of chemical shift data is indicated by gray bars. The residue numbering is consistent with that of Kabat et al. (*52*).

a direct result of the increased molecular mass and concomitant increase in rotational correlation time rather than any change in the local dynamic properties of CDR3.

Additional confirmation of the assignments was provided by the presence of sequential $^1H^N-^1H^N$ NOEs observed in a ^{15}N-edited NOESY-HSQC spectrum acquired on the sample containing $^{15}N/^{13}C/^2H$-labeled-V_H, perdeuterated-V_L, and excess unlabeled-EZ4 (Table 2). In addition to the sequential NOE correlations, all of the expected medium-range ($|i - j| < 5$) and long-range ($|i - j| \geq 5$) NOEs corresponding to $^1H^N-^1H^N$ distances of ≤ 4.5 Å in the Fv crystal structure were observed (where the expectation accounts for the unassigned amide resonances as well as resonance degeneracies and overlap with diagonal peaks). Observation of these NOEs indicates that the structure of the V_H-domain is essentially unchanged by SpA-domain binding.

Backbone V_H-resonance assignments for the free and EZ4-bound Fv-fragment are provided in the Supporting Information (Table S1). Plots showing deviations from random coil chemical shift values for assigned V_H-domain ^{13}CO, $^{13}C^\alpha$, and $^{13}C^\beta$ resonances in the free Fv and in the EZ4-bound state are also provided in the Supporting Information (Figures S3 and S4). The consensus chemical shift index values (*44*) for each state are shown in Figure 7. The chemical shift data for the bound state were corrected on the basis of ^2H-isotope-shifts measured for the free state. In general, the agreement between the secondary structure predicted using the CSIs and that observed in the crystal structure of the V_H-domain is good for the free state and for the assigned regions in the EZ4-bound state.

Chemical Shift Mapping of Binding Sites. Numerous protein-binding surfaces have been mapped through the observation of changes in chemical shifts between the free and bound states of the interacting partners (e.g., see refs *18*, *48*, and *49*). In cases of fast exchange, the positions of "bound" peaks can be determined readily by following resonance shifts during titration experiments. In cases of slow exchange, however, the bound peaks are frequently not assigned. Rather, resonances that show no apparent shift on complex formation (i.e., a peak is observed at the same position in both free and bound spectra) are tentatively assigned on the basis of the assigned spectrum of the free protein and are assumed to arise from regions of the protein outside the binding interface. The net changes in chemical shift of bound state resonances can also be estimated by measurement of minimum chemical shift changes (*50*). The precision of both approaches in defining binding sites can suffer in crowded spectra, however, due to unfortunate peak overlap. The surface described by chemical shift mapping is typically larger than the region in direct contact because residues on the edge of the binding site can experience changes in local environment induced by neighboring contact residues (*51*).

In the present study, backbone resonance assignments have been completed for both the free and bound members of the complex. The weighted net change in chemical shift for correlations observed in HNCO spectra acquired on EZ4 and the V_H-domain were calculated according to

$$\Delta\delta = [\Delta\delta_{^1H^N}{}^2 + 0.17\Delta\delta_{^{15}N}{}^2 + 0.39\Delta\delta_{^{13}CO}{}^2]^{1/2}$$

where $\Delta\delta$ is the combined chemical shift difference, and $\Delta\delta_{^1H^N}$, $\Delta\delta_{^{15}N}$, and $\Delta\delta_{^{13}CO}$ are the $^1H^N$, ^{15}N, and ^{13}CO chemical shift differences in parts per million, respectively, between the HNCO correlations for the free and bound proteins (*50*). The results of the calculation for EZ4 are shown in Figure 8A. An arbitrary $\Delta\delta_{cutoff}$ value of 0.13 ppm was selected to provide a reasonable degree of discrimination between V_H-domain-binding-site and non-binding-site residues. The deduced binding-site residues are shown mapped onto a model of EZ4 [based on the solution structure of E-domain (*11*)] in Figure 8B and include Asn21−Ala22, Gln24−Ile29, Ser31−Asp35, Ser37−Gln47, and Leu49−Asp51. This set of residues includes most of helices 2 and 3 in the solution structure of E-domain.

The results of the calculation for the V_H-domain are shown in Figure 9A. The V_H-residue numbering is consistent with that of Kabat et al. (*52*). As for EZ4, a 0.13 ppm $\Delta\delta_{cutoff}$ value was used to discriminate between EZ4-binding-site and non-binding-site residues; binding-site residues identified in this way include Gly15−Ser21, Ala23, Tyr56−Tyr59, Val63−Gly65, Thr68, Ala71, Asp72, and Tyr79−Asn82A, Leu82C, and Arg83. The large changes in backbone chemical shifts observed for Tyr56, Gly65, and Thr68 (Figure 9A) are most likely due to the proximity of the backbone nuclei to aromatic rings, rather than any gross conformational changes upon complex formation. V_H-domain residues Cys22, Ile69, Ser70, and Ser82B, which are sequentially adjacent to those that experienced significant chemical shift changes on binding, did not have observable amide signals in the EZ4-bound state. These resonances were observed in the free Fv; in this case, the differential broadening observed on binding suggests that these residues may also be part of the EZ4-binding site. The combined residue set is shown mapped onto the

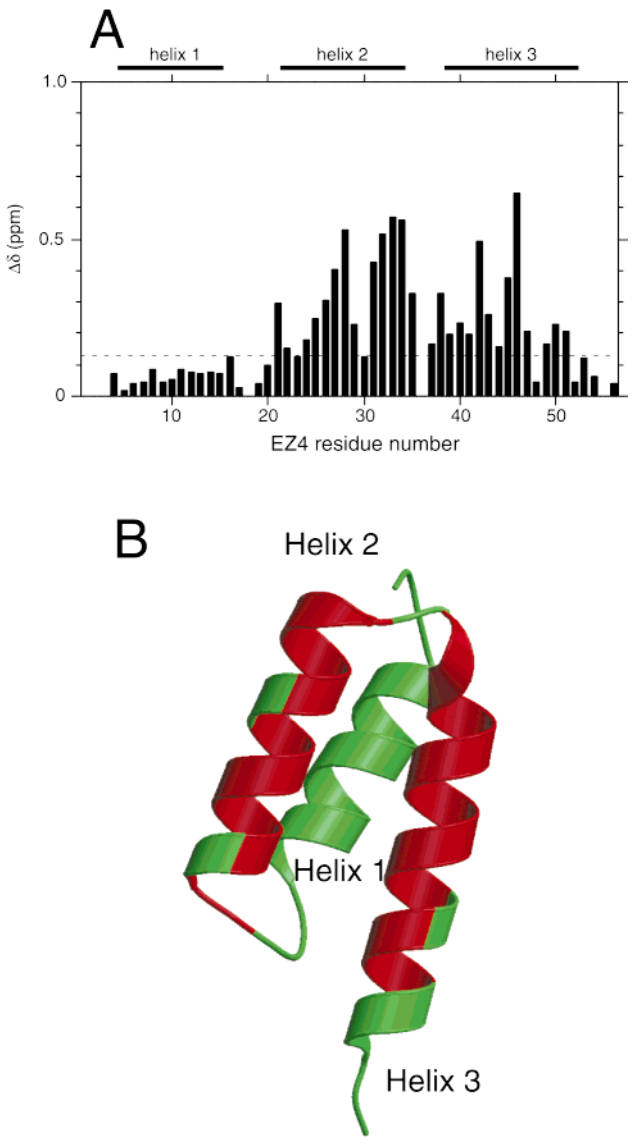

FIGURE 8: (A) Plot of weighted net change in EZ4 chemical shifts, $\Delta\delta$ (ppm), for $^{1}H^{N}$, ^{15}N, and ^{13}CO resonances in HNCO spectra of free and Fv-bound EZ4 (see text), versus residue number. Regions of secondary structure observed in the free domain are indicated at the top of the figure. The threshold used to differentiate between significantly perturbed and unperturbed residues, $\Delta\delta_{cutoff} = 0.13$ ppm, is shown as a dashed line. (B) Schematic representation of the E-domain solution structure [PDB accession code 1EDK (*11*)] illustrating EZ4-residues whose backbone $^{1}H^{N}$, ^{15}N, and ^{13}CO resonances are perturbed upon Fv binding. Residues that experience significant chemical shift changes on complex formation are colored red. This figure was generated using the program MOLSCRIPT (*63*).

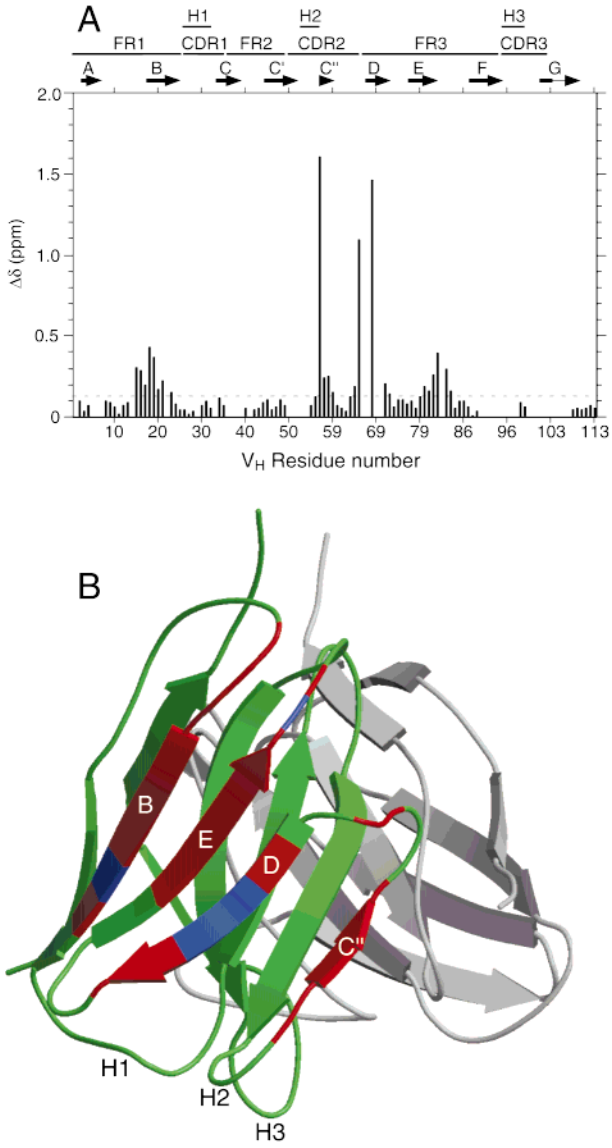

FIGURE 9: (A) Plot of weighted net change in V_H-chemical shift, $\Delta\delta$ (ppm), for $^{1}H^{N}$, ^{15}N, and ^{13}CO resonances in HNCO spectra of free and EZ4-bound Fv, versus residue number. The framework regions, complementarity determining regions, hypervariable regions, and secondary structure are indicated at the top of the figure. The threshold used to differentiate between significantly perturbed and unperturbed residues, $\Delta\delta_{cutoff} = 0.13$ ppm, is shown as a dashed line. (B) Schematic representation of the Fv crystal structure [PDB accession code 1FVC (*45*)] illustrating V_H-residues whose backbone $^{1}H^{N}$, ^{15}N, and ^{13}CO resonances are perturbed upon EZ4 binding. Residues that experience significant chemical shift changes on complex formation are colored red, while residues Cys22, Ile69, Ser70, and Ser82B, that were differentially broadened on complex formation, are colored violet. The V_L-domain is shown in gray. The antigen-binding site is at the bottom in this view. This figure was generated using the program MOLSCRIPT (*63*).

crystal structure of the V_H-domain (*45*) in Figure 9B and includes sections of strands B, D, and E of β-sheet 1 and strand C″ of β-sheet 2.

DISCUSSION

Description of the Mapped Binding Surfaces. The surface of SpA-domains involved in Fc-binding was shown previously to include residues from helices 1 and 2 (*15*). The deduced Fv-binding-surface (Figures 8B and 10) is distinct from the Fc-binding surface in that it includes residues from helices 2 and 3, consistent with the observation that SpA domains can bind both Fc and Fab simultaneously (*6*, *16*). The largely hydrophilic Fv-binding-surface comprises a small, central hydrophobic region bordered by charged and polar residues. The EZ4-binding surface of the V_H-domain (Figure 9B and 10) is also largely hydrophilic with a central hydrophobic patch bordered by several charged and polar residues. The hydrophilic nature of the SpA−Fv interface is in contrast to the predominantly hydrophobic interface observed in the SpA−Fc complex (*15*).

The SpA-binding-surface identified in the present study confirms previous speculation, based on V_H sequence

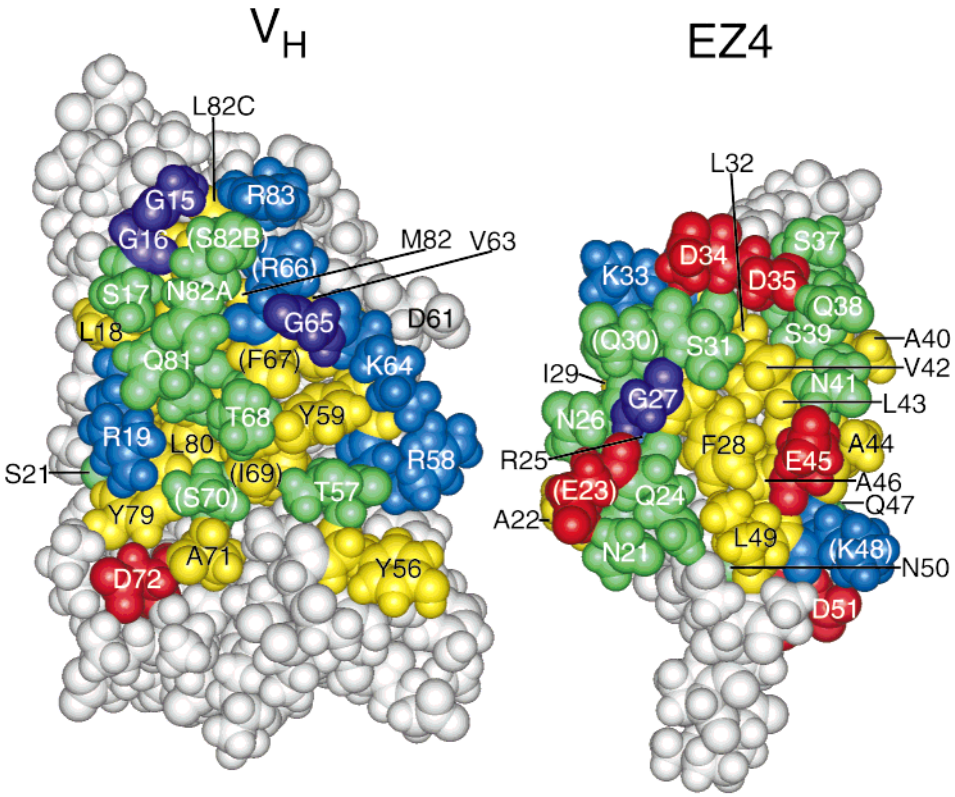

FIGURE 10: Space-filling representations of EZ4 [model based on the solution structure of E-domain; PDB accession code 1EDK (*11*)] (right) and the V_H-domain [from the Fv crystal structure; PDB accession code 1FVC (*45*)] (left), illustrating the deduced protein interaction sites. Proposed binding site residues are colored according to the following scheme: glycines, violet; hydrophobic, yellow; polar, green; basic, blue; acidic, red. Residues labeled in parentheses had resonances that were not observed in the complex or had net weighted backbone chemical shift changes on complex formation less than $\Delta\delta_{cutoff}$; they are included in the proposed binding site due to the proximity of their side chains to residues that did experience significant backbone chemical shift changes. This figure was produced using the program INSIGHT II (Molecular Simulations, Inc.).

analyses, that residues in FR1, the C-terminal section of CDR2, and FR3 of V_H3-domains are important for SpA binding (*19*−*22*). The present results are also in good agreement with those of Riechmann and Davies (*18*), although they concluded that chemical shift perturbations in β-strand C″ were likely due to indirect effects rather than direct contact. While this remains a formal possibility, we believe that the complementarity observed in the two surfaces mapped in Figure 10, together with the results of functional studies (see discussion below), argues strongly for this region of CDR2 to be included in the SpA-binding site. An exception might be Tyr56, which is located on the edge of the mapped binding surface (Figure 10) and may not necessarily contact EZ4 directly; the side chain of this conserved CDR2 residue has been shown previously to contribute ~1 kcal mol^{-1} to HER2 binding (*53*). Note, however, that no part of any V_H-domain hypervariable loop is included in the proposed contact surface, consistent with the fact that SpA-domains are capable of binding highly diverse V_H3-sequences and do not usually affect antigen binding.

Complementarity of the Mapped Binding Surfaces. Inspection of the binding surfaces (Figure 10) reveals apparent charge complementarity that suggests a possible binding orientation for the two domains with respect to each another. Figure 10 shows an "open-book" representation of this likely binding mode. Such a binding mode would allow several salt-bridges to form at the interface of the complex: (EZ4-residue/Fv-residue) Asp34 or Asp35/Arg66 or Arg83; Glu45/Arg19; Glu23/Arg58; and Lys48/Asp72. This set of interactions leaves Lys64 as the only V_H-residue within the binding surface lacking a compensating charge within the EZ4 V_H-binding surface; this residue interacts with Asp61 in the crystal structure of the Fv. The proposed electrostatic interactions could occur simultaneously with little change in the conformations of either EZ4 or Fv upon complex formation, as expected based on the NOE and CSI analyses of the free and bound proteins. The binding surfaces are relatively flat, although closer inspection reveals several shallow grooves and ridges that also provide shape complementarity consistent with the binding orientation suggested on the basis of the electrostatic interactions.

The proposed binding orientation offers an explanation for the greatly reduced V_H-binding affinity observed for Z-domain [G27A mutant of B-domain (*14*)] in that the presence of a methyl group at position 27 would lead to a steric clash with Tyr59 and/or Gly65, residues that are completely conserved in germ-line V_H3-sequences.

V_H-Segment Binding Specificity of SpA-Domains. Tomlinson et al. estimate the number of human germ-line V_H-gene segments to be 83, of which 29 are classified as belonging to family 3 (*54*). Variable region binding by SpA-repeats is known to involve preferentially a select subset of the V_H3-family of gene segments (*4*−*7*). Analysis of potential interactions between the binding surfaces identified in the present study, that follow necessarily from the proposed binding orientation in the EZ4−Fv complex (Figure 10), provides a basis for speculation on the observed specificity

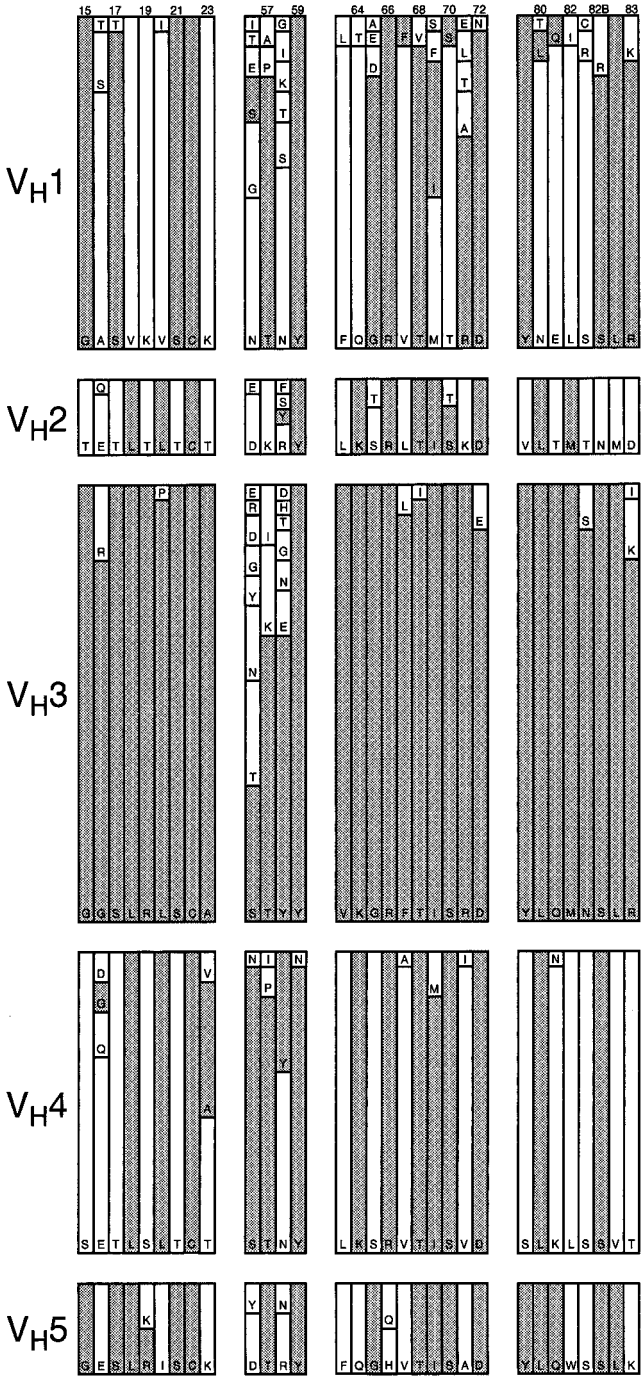

FIGURE 11: Alignment of the amino acid composition for 82 germ-line V_H-sequences (from V_H-families 1−5) within the four regions identified as being involved in EZ4 binding to the V_H3-domain of Hu4D5−8 (see Figure 9B). The length of each bar is proportional to the frequency of occurrence of a particular amino acid type within the 82 sequences analyzed. Identity with the consensus V_H3 sequence is indicated by shading. The germ-line V_H-sequences are from Tomlinson et al. (*54*).

of binding of SpA-domains for certain V_H-domains. A comparison of the amino acid sequences of germ-line V_H-families 1−5 (*54*), for the regions corresponding to those involved in SpA binding to V_H3, is given in Figure 11.

The proposed binding orientation is consistent with the results of Randen et al. (*23*), who observed that four of five non-SpA-binding V_H3-domains studied contain acidic amino acids at positions 57 or 58. In the proposed mode of binding, negative charge at these positions would lead to unfavorable electrostatic interactions with SpA residues 22 or 23 (note that native SpA domains A−D have glutamate at position 22 while A, B, C, and E also have either aspartate or glutamate at position 23). Furthermore, these authors showed that introducing a lysine residue at V_H-position 57 restored SpA binding.

Arg19 is conserved strictly in germ-line V_H3-sequences but is substituted conservatively with lysine in V_H1-germ-line sequences and in 50% of V_H5-germ-line sequences; in contrast, threonine and serine are conserved strictly at this position in V_H2- and V_H4-germ-line sequences, respectively (Figure 11). Additionally, a lysine or arginine is found at position 83 in V_H1-, V_H3-, and V_H5-germ-line sequences; this residue is always an aspartate or threonine in V_H2- and V_H4-germ-line sequences, respectively (Figure 11). The loss of favorable electrostatic interactions between V_H-residues 19 and 83 and SpA-residues 45 and 34/35, respectively, potentially explains the lack of SpA-domain binding in V_H-families 2 and 4. The lack of SpA-domain binding exhibited by V_H1- and V_H5-germ-line sequences might be explained in part by differences in sequence between these families and V_H-family 3 in FR1 and FR3. Germ-line V_H3-sequences contain a conserved glycine at position 16 in contrast to all other germ-line V_H-sequences. A nonglycine substitution at position 16 might easily promote a steric clash with, and in this way perturb binding to, a SpA-domain. Substitution of this glycine with an acidic amino acid in V_H-5 and the majority of V_H-4-germ-line sequences would likely introduce an unfavorable electrostatic-interaction with the conserved SpA residue Asp35. The FR3 sequence from residues 79−82 in germ-line V_H3-sequences is conserved absolutely; this sequence differs in at least two positions in the other germ-line V_H-families (Figure 11). These substitutions may also result in additional unfavorable contributions to the SpA-domain/V_H-domain interaction in non-SpA-domain binding V_H-sequences.

CONCLUSION

The SpA and V_H-domain binding surfaces identified in this study and the relative binding orientations proposed on the basis of the charge complementarity observed between these binding surfaces are consistent with available mutagenesis and sequence data from both SpA and V_H-domains. The fact that the Fc- and Fab-binding surfaces on SpA-domains appear to be distinct and nonoverlapping correlates with the observation of noncompetitive Fab and Fc binding by these domains. The ability of SpA-domains to utilize both binding surfaces simultaneously would appear to enhance the ability of protein A to cross-link Ig sequences, thus enhancing the antigenicity of *S. aureus*.

ACKNOWLEDGMENT

We thank Dorothy Reilly for providing the cell lines used to produce the protein utilized in this study, Steven Bass and Jill Heinrich for providing the V_H- and V_L-plasmids, Len Presta, and Eugene Zhukovsky for assistance in creating and characterizing the EZ4-mutant of E-domain, Robert Kelley for determining the binding constants for the E-Fv and EZ4−Fv complexes, and James Bourell for mass spectrometry analysis.

REFERENCES

1. Uhlén, M., Guss, B., Nilsson, B., Gatenbeck, S., Philipson, L., and Lindberg, M. (1984) *J. Biol. Chem. 259*, 1695−1702.
2. Nardella, F. A., Teller, D. C., Barber, C. V., and Mannik, M. (1985) *J. Exp. Med. 162*, 1811−24.
3. Vidal, M. A., and Conde, F. P. (1985) *J. Immunol. 135*, 1232−1238.
4. Sasso, E. H., Silverman, G. J., and Mannik, M. (1989) *J. Immunol. 142*, 2778−2783.
5. Sasso, E. H., Silverman, G. J., and Mannik, M. (1991) *J. Immunol. 147*, 1877−1883.
6. Roben, P. W., Salem, A. N., and Silverman, G. J. (1995) *J. Immunol. 154*, 6437−6445.
7. Jansson, B., Uhlén, M., and Nygren, P.-A. (1998) *FEMS Immunol. Med. Microbiol. 20*, 69−78.
8. Romagnani, S., Giudizi, M. G., Del Prete, G., Maggi, E., Biagiotti, R., Almerigogna, F., and Ricci, M. (1982) *J. Immunol. 129*, 596−602.
9. Kozlowski, L. M., Soulika, A. M., Silverman, G. J., Lambris, J. D., and Levinson, A. I. (1996) *J. Immunol. 157*, 1200−1206.
10. Kozlowski, L. M., Li, W., Goldschmidt, M., and Levinson, A. I. (1998) *J. Immunol. 160*, 5246−5252.
11. Starovasnik, M. A., Skelton, N. J., O'Connell, M. P., Kelley, R. F., Reilly, D., and Fairbrother, W. J. (1996) *Biochemistry 35*, 15558−15569.
12. Gouda, H., Torigoe, H., Saito, A., Sato, M., Arata, Y., and Shimada, I. (1992) *Biochemistry 31*, 9665−9672.
13. Tashiro, M., Tejero, R., Zimmerman, D. E., Celda, B., Nilsson, B., and Montelione, G. T. (1997) *J. Mol. Biol. 272*, 573−590.
14. Nilsson, B., Moks, T., Jansson, B., Abrahmsén, L., Elmblad, A., Holmgren, E., Henrichson, C., Jones, T. A., and Uhlén, M. (1987) *Protein Eng. 1*, 107−113.
15. Deisenhofer, J. (1981) *Biochemistry 20*, 2361−2370.
16. Starovasnik, M. A., O'Connell, M. P., Fairbrother, W. J., and Kelley, R. F. (1999) *Protein Sci. 8*, 1423−1431.
17. Young, W. W., Tamura, Y., Wolock, D. M., and Fox, J. W. (1984) *J. Immunol. 133*, 3163−3166.
18. Riechmann, L., and Davies, J. (1995) *J. Biomol. NMR 6*, 141−152.
19. Hillson, J. L., Karr, N. S., Oppliger, I. R., Mannik, M., and Sasso, E. H. (1993) *J. Exp. Med. 178*, 331−336.
20. Sasano, M., Burton, D. R., and Silverman, G. J. (1993) *J. Immunol. 151*, 5822−5839.
21. Hakoda, M., Hayashimoto, S., Yamanaka, H., Terai, C., Kamatani, N., and Kashiwazaki, S. (1994) *Clin. Immunol. Immunopathol. 72*, 394−401.
22. Hakoda, M., Kamatani, N., Hayashimoto-Kurumada, S., Silverman, G. J., Yamanaka, H., Terai, C., and Kashiwazaki, S. (1996) *J. Immunol. 157*, 2976−2981.
23. Randen, I., Potter, K. N., Li, Y., Thompson, K. M., Pascual, V., Førre, Ø., Natvig, J. B., and Capra, J. D. (1993) *Eur. J. Immunol. 23*, 2682−2686.
24. Potter, K. N., Li, Y., and Capra, J. D. (1996) *J. Immunol. 157*, 2982−2988.
25. Carter, P., Presta, L., Gorman, C. M., Ridgway, J. B. B., Henner, D., Wong, W. L. T., Rowland, A. M., Kotts, C., Carver, M. E., and Shepard, H. M. (1992) *Proc. Natl. Acad. Sci. U.S.A. 89*, 4285−4289.
26. Chang, C. N., Rey, M., Bochner, B., Heyneker, H., and Gray, G. (1987) *Gene 55*, 189−196.
27. Reilly, D., and Fairbrother, W. J. (1994) *J. Biomol. NMR 4*, 459−462.
28. Wishart, D. S., Bigam, C. G., Yao, J., Abildgaard, F., Dyson, H. J., Oldfield, E., Markley, J. L., and Sykes, B. D. (1995) *J. Biomol. NMR 6*, 135−140.
29. Cavanagh, J., Fairbrother, W. J., Palmer, A. G., III, and Skelton, N. J. (1995) *Protein NMR spectroscopy: principles and practice*, Academic Press, San Diego.
30. Marion, D., Ikura, M., Tschudin, R., and Bax, A. (1989) *J. Magn. Reson. 85*, 393−399.
31. Grzesiek, S., and Bax, A. (1993) *J. Am. Chem. Soc. 115*, 12593−12594.
32. Mori, S., Abeygunawardana, C., O'Neil Johnson, M., and van Zijl, P. C. M. (1995) *J. Magn. Reson. B 108*, 94−98.
33. Driscoll, P. C., Clore, G. M., Beress, L., and Gronenborn, A. M. (1989) *Biochemistry 28*, 2178−2187.
34. Talluri, S., and Wagner, G. (1996) *J. Magn. Reson. B 112*, 200−205.
35. Kay, L. E., Keifer, P., and Saarinen, T. (1992) *J. Am. Chem. Soc. 114*, 443−450.
36. Muhandiram, D. R., and Kay, L. E. (1994) *J. Magn. Reson. B 103*, 203−216.
37. Pervushin, K., Riek, R., Wider, G., and Wüthrich, K. (1997) *Proc. Natl. Acad. Sci. U.S.A. 94*.
38. Salzmann, M., Pervushin, K., Wider, G., Senn, H., and Wüthrich, K. (1998) *Proc. Natl. Acad. Sci. U.S.A. 95*, 13585−13590.
39. Loria, J. P., Rance, M., and Palmer, A. G., III. (1999) *J. Magn. Reson. 141*, 180−184.
40. Shaka, A. J., Keeler, J., Frenkiel, T., and Freeman, R. (1983) *J. Magn. Reson. 52*, 335−338.
41. Shaka, A. J., Barker, P. B., and Freeman, R. (1985) *J. Magn. Reson. 64*, 547−552.
42. McCoy, M. A., and Mueller, L. (1992) *J. Am. Chem. Soc. 114*, 2108−2112.
43. McCoy, M. A., and Mueller, L. (1992) *J. Magn. Reson. 98*, 674−679.
44. Wishart, D. S., and Sykes, B. D. (1994) *J. Biomol. NMR 4*, 171−180.
45. Eigenbrot, C., Randal, M., Presta, L., Carter, P., and Kossiakoff, A. A. (1993) *J. Mol. Biol. 229*, 969−995.
46. Freund, C., Ross, A., Plückthun, A., and Holak, T. A. (1994) *Biochemistry 33*, 3296−3303.
47. Takahashi, H., Suzuki, E., Shimada, I., and Arata, Y. (1992) *Biochemistry 31*, 2464−2468.
48. Chen, Y., Reizer, J., Saier, M. H., Jr., Fairbrother, W. J., and Wright, P. E. (1993) *Biochemistry 32*, 32−37.
49. van Nuland, N. A. J., Kroon, G. J. A., Dijkstra, K., Wolters, G. K., Scheek, R. M., and Robillard, G. T. (1993) *FEBS Lett 315*, 11−15.
50. Farmer, B. T., II, Constantine, K. L., Goldfarb, V., Friedrichs, M. S., Wittekind, M., Yanchunas, J. J., Robertson, J. G., and Mueller, L. (1996) *Nat. Struct. Biol. 3*, 995−997.
51. Spitzfaden, C., Weber, H. P., Braun, W., Kallen, J., Wider, G., Widmer, H., Walkinshaw, M. D., and Wüthrich, K. (1992) *FEBS Lett 300*, 291−300.
52. Kabat, E. A., Wu, T. T., Perry, H. M., Gottesman, K. S., and Foeller, C. (1991) *Sequences of proteins of immunological interest*, 5th ed., Public Health Service, NIH, Washington DC.
53. Kelley, R. F., and O'Connell, M. P. (1993) *Biochemistry 32*, 6828−6835.
54. Tomlinson, I. M., Walter, G., Marks, J. D., Llewelyn, M. B., and Winter, G. (1992) *J. Mol. Biol. 227*, 776−798.
55. Bax, A., Ikura, M., Kay, L. E., Torchia, D. A., and Tschudin, R. (1990) *J. Magn. Reson. 86*, 304−318.
56. Grzesiek, S., and Bax, A. (1992) *J. Magn. Reson. 96*, 432−440.
57. Montelione, G. T., Lyons, B. A., Emerson, D. A., and Tashiro, M. (1992) *J. Am. Chem. Soc. 114*, 10974−10975.
58. Logan, T. M., Olejniczak, E. T., Xu, R. X., and Fesik, S. W. (1993) *J. Biomol. NMR 3*, 225−231.
59. Yamazaki, T., Lee, W., Revington, M., Mattiello, D. L., Dahlquist, F. W., Arrowsmith, C. H., and Kay, L. E. (1994) *J. Am. Chem. Soc. 116*.
60. Yamazaki, T., Lee, W., Arrowsmith, C. H., Muhandiram, D. R., and Kay, L. E. (1994) *J. Am. Chem. Soc. 116*, 11655−11666.
61. Clubb, R. T., Thanabal, V., and Wagner, G. (1992) *J. Magn. Reson. 97*, 213−217.
62. Marion, D., Kay, L. E., Sparks, S. W., Torchia, D. A., and Bax, A. (1989) *J. Am. Chem. Soc. 111*, 1515−1517.
63. Kraulis, P. (1991) *J. Appl. Crystallogr. 24*, 946−950.

BI9920174